

This is a repository copy of *Lytic xylan oxidases from wood-decay fungi unlock biomass degradation*.

White Rose Research Online URL for this paper:

<https://eprints.whiterose.ac.uk/id/eprint/126886/>

Version: Accepted Version

Article:

Couturier, Marie, Ladevèze, Simon, Sulzenbacher, Gerlind et al. (19 more authors) (2018) Lytic xylan oxidases from wood-decay fungi unlock biomass degradation. NATURE CHEMICAL BIOLOGY. pp. 306-310. ISSN: 1552-4450

<https://doi.org/10.1038/nchembio.2558>

Reuse

Items deposited in White Rose Research Online are protected by copyright, with all rights reserved unless indicated otherwise. They may be downloaded and/or printed for private study, or other acts as permitted by national copyright laws. The publisher or other rights holders may allow further reproduction and re-use of the full text version. This is indicated by the licence information on the White Rose Research Online record for the item.

Takedown

If you consider content in White Rose Research Online to be in breach of UK law, please notify us by emailing eprints@whiterose.ac.uk including the URL of the record and the reason for the withdrawal request.

Lytic xylan oxidases from wood-decay fungi unlock biomass degradation

Marie Couturier^{1,*}, Simon Ladevèze^{1,*}, Gerlind Sulzenbacher^{2,3}, Luisa Ciano⁴, Mathieu Fanuel⁵, Céline Moreau⁵, Ana Villares⁵, Bernard Cathala⁵, Florence Chaspoul⁶, Kristian E. Frandsen¹, Aurore Labourel¹, Isabelle Herpoël-Gimbert¹, Sacha Grisel¹, Mireille Haon¹, Nicolas Lenfant², Hélène Rogniaux⁵, David Ropartz⁵, Gideon Davies⁴, Marie-Noëlle Rosso¹, Paul H. Walton⁴, Bernard Henrissat^{2,3,7}, Jean-Guy Berrin^{1,**}

¹INRA, Aix Marseille Univ., Biodiversité et Biotechnologie Fongiques (BBF), UMR1163, F-13009 Marseille, France

²Architecture et Fonction des Macromolécules Biologiques (AFMB), CNRS, Aix-Marseille Univ., F-13009 Marseille, France

³INRA, USC1408 Architecture et Fonction des Macromolécules Biologiques (AFMB), F-13009 Marseille, France

⁴Department of Chemistry, University of York, York, UK, YO10 5DD

⁵INRA, Unité de Recherche Biopolymères Interactions Assemblages (BIA), F-44316 Nantes, France

⁶IMBE Aix Marseille Univ., IRD CNRS UAPV, Faculté de Pharmacie, F-13005 Marseille, France.

⁷Department of Biological Sciences, King Abdulaziz University, Jeddah, Saudi Arabia

*These authors contributed equally to this work

**Correspondence and request to materials should be addressed to J.G.B.

(jean-guy.berrin@inra.fr)

Abstract

Wood biomass is the most abundant feedstock envisioned for the development of modern biorefineries. However, the cost-effective conversion of this form of biomass to commodity products is limited by its resistance to enzymatic degradation. Here we describe a new family of fungal lytic polysaccharide monooxygenases (LPMOs) prevalent amongst white-rot and brown-rot basidiomycetes, which is active on xylans - a recalcitrant polysaccharide abundant in wood biomass. Two AA14 LPMO members from the white-rot fungus *Pycnoporus coccineus* significantly increase the efficiency of wood saccharification through oxidative cleavage of highly refractory xylan-coated cellulose fibers. The discovery of this unique enzyme activity advances our knowledge on the degradation of woody biomass in nature and offers an innovative solution to improve enzyme cocktails for biorefinery applications.

Introduction

Wood is the most abundant organic source of biomass on Earth, with an annual production of about 5.64×10^{10} tons of carbon¹. Its widespread nature has allowed humans to use it in many contexts, most notably as a building material due to its exceptional mechanical properties and resistance to decay. In bio-based industries, the utilization of wood is taking on a new importance as it constitutes the most promising source for advanced biofuels and plant-derived products. Notwithstanding its potential, however, the cost-effective conversion of woody feedstocks is limited by a single key factor, the recalcitrance of the lignocellulosic matrix to degradation by enzyme cocktails². To overcome this recalcitrance, biorefineries utilize energy-demanding pretreatment processes to solubilize the inaccessible biomass components before enzymatic saccharification. The recalcitrant fraction reflects its heteroxylan content which is known to be particularly resistant to xylanases due to extensive decoration and because these xylans can adopt a flat conformation with their chains solidly adhering *via* hydrogen-bonds to the surface of cellulose microfibrils^{3,4}. Finding sustainable means of overcoming this resistance to degradation is one of the main challenges faced by modern biorefineries. Indeed, the xylan problem is so severe that consideration is being given to engineering energy crops modified to contain fewer recalcitrant xylans⁵.

In nature, fungi play a vital role in the terrestrial carbon cycle and dominate wood decomposition in boreal forests⁶. Wood-decaying basidiomycetes classified as white-rot and brown-rot fungi, naturally degrade cellulose and hemicelluloses using a large diversity of carbohydrate-active enzymes (CAZymes; www.cazy.org)⁷ and Fenton-type chemistry⁸. In this context, understanding of plant-cell wall deconstruction was recently overturned by the discovery of lytic polysaccharide monooxygenases (LPMOs) enzymes which cleave polysaccharides through an

oxidative as opposed to hydrolytic mechanism⁹⁻¹¹. Such is their importance, that industrial enzyme mixtures for the conversion of agricultural residues to biofuels now incorporate cellulose-active LPMOs¹², helping biorefineries move towards environmental and economic sustainability. Despite the significant efficiencies that LPMOs have brought to biomass degradation, industrial enzyme cocktails are still unable to degrade woody biomass completely and there is a major need to identify new enzymes capable of effecting this breakdown. From this perspective, there are three fungal LPMO families (termed AA9, AA11 and AA13 in the CAZy classification)⁷, which were discovered from genome sequences by virtue of their modular structure where the catalytic LPMO domain is sometimes appended to known substrate-targeting carbohydrate-binding modules (CBMs). Each fungal LPMO family is associated with the oxidative cleavage of distinct polysaccharides with AA9 acting mainly on cellulose and xyloglucan¹⁰, AA11 on chitin¹³ and AA13 on starch^{14,15}; a solely xylan-acting LPMO is conspicuous by its absence.

Using comparative post-genomic approaches among fungal wood decayers, we identified the existence of a previously unknown family of LPMO. This new family to be termed AA14 in the CAZy classification differs phylogenetically and structurally from the previous AA9, AA10, AA11 and AA13 families. The first characterized members from the white-rot basidiomycete fungus *Pycnoporus coccineus* target xylan chains covering wood cellulose fibers thus unlocking the enzymatic degradation of wood biomass.

Results

Discovery of the AA14 family among fungal wood decayers

The white-rot basidiomycete *Pycnoporus coccineus* is an efficient degrader of both hardwood and softwood¹⁶. While studying the effect of different types of biomass on *P. coccineus* growth using transcriptomics and secretomics, we identified a gene encoding a protein of unknown function that was highly up-regulated on pine and poplar as compared to control¹⁶. The corresponding protein (JGI ID 1372210; GenBank ID #KY769370) was secreted only during growth on pine and poplar suggesting a role in wood decay. A BLAST search against public sequence databases identified more than 300 proteins with significant similarity to #KY769370 from *P. coccineus*, many of which from well-known saprotrophic fungi. Sequence alignment revealed a conserved N-terminal histidine (**Supplementary Fig. 1**), commensurate with a copper-binding histidine brace active site¹⁰, which is a hallmark of known LPMOs. A phylogenetic analysis shows that the newly identified sequences strongly cluster together with high bootstrap values and are very distant from AA9, AA10, AA11 and AA13 sequences (**Supplementary Fig. 2**), thereby defining a new LPMO family designated AA14 in the CAZy database. AA14 members are found in all well-known white-rot (*Pleurotus ostreatus*, *Phanerochaete chrysosporium*, *Trametes versicolor*) and brown-rot (*Serpula lacrymans*, *Coniophora puteana*, *Postia placenta*) basidiomycetes and in some wood-inhabitants ascomycetes within the *Xylariaceae* and *Hypocreaceae* families. A slight gene family expansion is observed in wood-decaying basidiomycetes (average number per species 3.35 in basidiomycetes and 1.28 in ascomycetes) (**Fig. 1; Supplementary Data Set 1**). None of the AA14 members identified in fungal genomes harbors a carbohydrate-binding module (CBM)

explaining why this family was not previously discovered together with AA11 and AA13 through the “module walk” approach^{13,15}.

Expression and biochemical characterization of *PcAA14*

Two *P. coccineus* proteins, *PcAA14A* (#KY769369) and *PcAA14B* (#KY769370), displaying 65% sequence identity were produced to high yield in *Pichia pastoris*, purified to homogeneity and biochemically characterized (**Supplementary Table 1; Supplementary Fig. 3 and 4**). We confirmed the correct processing of the native signal peptide, which exposed the N-terminal histidine residue at position 1 in the mature polypeptide chain (**Supplementary Table 1**). Mass spectrometry analyses revealed that both proteins contained ~ one copper atom per protein molecule and treatment with EDTA led to partial apo forms (~0.1 copper atom per protein molecule). *PcAA14A* and *PcAA14B* were both able to produce hydrogen peroxide in the presence of ascorbate, cysteine or gallate as electron donors (**Supplementary Table 2**).

Crystal structure of *PcAA14*

The structure of *PcAA14B* was solved by multiple-wavelength anomalous dispersion data recorded at the gadolinium edge, and refined at 3.0 Å resolution. The core of the protein folds into a largely antiparallel immunoglobulin-like β-sandwich (**Fig. 2a**), a fold globally similar to that seen in LPMOs from other families. The active site of *PcAA14B* constituted by His1, His99 and Tyr176 forming the canonical histidine brace is exposed at the surface (**Fig. 2b**). In contrast to the flat substrate-binding surfaces observed in AA9 LPMOs¹⁷, the *PcAA14B* surface has a rippled shape with a clamp formed by two prominent surface loops (**Supplementary Fig. 5**). Both loops are located in the N-terminal half of *PcAA14B*, and are equivalent to the L2 and L3 loop regions in AA9 LPMOs. Conventionally, the N-terminal part of AA9 LPMOs upstream of the L2 loop region makes up a β-strand segment (single β-strand or a β-hairpin). No equivalent

β -strands are found in the *PcAA14B* structure, which, in contrast, forms loop segments immediately after the N-terminal His (**Supplementary Fig. 5**). The *PcAA14B* structure also reveals a cystine (Cys67-Cys90) in the L3-equivalent region, which borders an extension not present in AA9 LPMOs (**Supplementary Fig. 5**). It is highly interesting to note that the two loops making up the clamp in *PcAA14B* correspond to modified L2 and L3 loop regions, as these have been shown to be involved in LPMO-substrate interactions¹⁷. For AA9 LPMOs a conserved Tyr has been shown to be involved in substrate interactions at the active site surface¹⁷. Interestingly, *PcAA14B* possesses equally a conserved tyrosine residue at the edge of the substrate-binding surface, Tyr240, albeit located on a different loop region, which could potentially make substrate interactions. Overall the crystal structure of *PcAA14B* reveals novel features within its putative substrate binding site, which may suggest differences in terms of substrate specificity compared to known LPMOs.

EPR spectroscopic analysis of the copper site of *PcAA14*

Multi-frequency Electron Paramagnetic Resonance (EPR) analysis was carried out on both *PcAA14A* and *PcAA14B* to determine the nature of the copper active site (Figure 2C; **Supplementary Fig. 6**). The spin Hamiltonian parameters (**Supplementary Table 3**) displayed axial parameters ($g_x \approx g_y < g_z$) with a $d(x^2-y^2)$ SOMO, placing the copper active site squarely within a type 2 Peisach-Blumberg classification¹⁸. Simulations required the addition of two ($I=1$) nitrogen atoms (coupling in the range of 30 to 36 MHz), as would be expected from the coordinating histidine side chains. Overall, these spin-Hamiltonian parameters are similar to those obtained for AA9 LPMOs confirming the presence of the copper(II) ion within the histidine brace coordination environment¹⁹. These data support the hypothesis that *PcAA14s* display LPMO characteristics and that copper is their native metal cofactor.

Substrate specificity of *PcAA14*

Activity assays were initially carried out with *PcAA14A* and *PcAA14B* on a wide range of polysaccharides including cellulose and xylans in the presence of ascorbic acid, which is widely used as electron donor for LPMOs. Using standardized methods previously employed to characterize AA9 LPMOs²⁰, no activity could be detected on these polysaccharides. Next, we performed saccharification assays on pretreated biomass including poplar, pine and wheat straw using a *Trichoderma reesei* CL847 cocktail mainly composed of cellulases and xylanases²¹. A boost of glucose release from poplar and pine was observed upon addition of either of the AA14 enzymes to the cocktail (**Fig. 3a**). When the reactions were conducted in absence of a reductant the boost effect was maintained (**Supplementary Fig. 8**), suggesting that one of the components from the biomass (e.g. lignin) may act as an electron donor²². This improvement in glucose release was dose-dependent yielding up to ~100% increase on pretreated softwood (**Fig. 3b**). However, no significant boost was observed on wheat straw (**Supplementary Fig. 8**), which differs in terms of hemicellulose composition compared to wood, indicating that AA14 enzymes specifically target one of the components of woody biomass. In a finding with important consequences for biorefinery use of woody biomass as feedstock, the *T. reesei* CL847 cocktail enriched in AA9 LPMO acting on cellulose was also boosted by *PcAA14A*, suggesting that AA9 and AA14 enzymes may act on different regions within the lignocellulosic matrix (**Supplementary Fig. 8**). Because AA14 members do not harbor any CBM module, we artificially attached a fungal CBM1 module targeting crystalline cellulose to *PcAA14A*. The resulting modular *PcAA14A*-CBM1 enzyme performed less efficiently than the catalytic module alone (**Supplementary Fig. 8**), suggesting that AA14 enzymes may not require specific binding to the flat crystalline cellulose surface.

To discern which polymer was attacked by AA14 enzymes, we used birchwood cellulosic fibers, consisting of 79% cellulose and 21% xylan, as a substrate. After incubation with *PcAA14A* or *PcAA14B*, wood fibers were disrupted (**Fig. 4a**) uncovering cellulose structures visualized at different scales using transmission electron microscopy and atomic force microscopy (**Supplementary Fig. 9**). These observations suggest a weakening of the cohesive forces that link the wood fibers together in a manner similar to that previously described with AA9 enzymes²³. Samples treated with AA14 enzymes were further analyzed using solid-state Cross-Polarization Magic Angle Spinning ¹³C Nuclear Magnetic Resonance (¹³C CP/MAS NMR). The impact of AA14 enzymes on the fibers was different to that recently observed for AA9 LPMOs²³. In the case of *PcAA14* enzymes, no meaningful change was observed on cellulose signals (**Fig. 4b**; **Supplementary Fig. 10**). Interestingly, however, significant changes in signal areas corresponding to hemicelluloses located at 101 ppm and 82 ppm were observed when the NMR spectra were deconvoluted in the C-1 and the C-4 regions (**Supplementary Fig. 10**). These results suggest that AA14 enzymes act on xylans bound to cellulose, which have a rigidity and a conformation similar to that of the underlying cellulose chains⁴. The specific attack of *PcAA14* on xylan substrates differentiates this new class of enzymes from all other LPMOs^{24,25}, none of which has previously been reported to oxidize xylan in such a selective and efficient manner.

To further substantiate the idea that AA14 enzymes act on xylan bound to cellulose, we performed synergy assays of AA14 enzymes in combination with a fungal GH11 xylanase using birchwood cellulosic fibers. Addition of *PcAA14A* to a GH11 xylanase significantly increased by 40% the release of xylo-oligomers from birchwood cellulosic fibers (Figure 4C; **Supplementary Fig. 11**). Additionally, no improvement of xylan conversion was observed on

birchwood cellulosic fibers when the xylanase was combined with a cellulose-acting AA9 LPMO (**Fig. 4c**).

We further investigated the nature of soluble products generated after synergistic action of *PcAA14A* and the GH11 xylanase. Using ionic chromatography, a range of oligosaccharides eluted at similar retention time to C1-oxidized oligosaccharides (**Supplementary Fig. 11**). Mass spectrometry analyses performed on the same samples allowed the identification of several putative oxidative species with masses corresponding to C1-oxidized xylo-oligosaccharides substituted with glucuronic acid (X₃MeGlcA, X₄MeGlcA, X₅MeGlcA) (**Supplementary Fig. 12**). The structure of the C1-oxidized xylo-oligosaccharides with an aldonic acid on the reducing end (**Fig. 4d**) was confirmed by fragmentation of the species observed at 429 *m/z* by tandem MS (MS/MS) (**Supplementary Fig. 12**). The identification of oxidative products demonstrates that AA14 enzymes are LPMOs.

Discussion

Our findings that xylans are susceptible to AA14 oxidative cleavage only when adsorbed onto crystalline cellulose and not when in solution are supported by reports that showed that xylans exist in different contexts within the cell wall^{4,26}. Recalcitrant xylans bound to cellulose microfibrils display a two-fold screw axis conformation aligned parallel to the cellulose chain direction⁴ that is compatible with the proper orientation of the carbohydrate H1 and H4 atoms with respect to the LPMO catalytic center²². Unravelling the substrate specificity of AA14s has been challenging as these enzymes are not active on xylans in solution most probably due to the three-fold helical screw conformation of the substrate²⁷. Using multidisciplinary approaches, we reveal that AA14 LPMOs probably target specifically the protective shield made by heteroxylans

that cover cellulose microfibrils in wood. The conformation of xylan in this context contributes to wood recalcitrance and glycoside hydrolases are not able to access such a sterically restricted substrate. The cleavage of these rare motifs by AA14 LPMOs unlocks the accessibility of xylan and cellulose chains to glycoside hydrolases therefore improving the overall saccharification of woody biomass. These results not only greatly enhance our knowledge of wood superstructure, they also contribute to understand and better exploit biomass deconstruction by fungal saprotrophs.

Acknowledgements. We thank the European Synchrotron Radiation Facility (Grenoble), and the synchrotron Soleil (Gif-sur-Yvette) for beam time allocation and assistance. We thank S. Tapin for providing cellulose fibers, E. Bonnin and J. Vigouroux for compositional analyses, G. Toriz and P. Gatenholm for providing purified wood xylan, L. Foucat and X. Falourd for their valued assistance with treatments of the NMR data, E. Perrin for the excellent technical support for TEM images, B. Seantier for the access and assistance to AFM facilities, D. Hartmann and E. Bertrand for their help with enzyme production in bioreactor, and D. Navarro and G. Anasontzis for insightful discussions. MC was funded by a Marie Curie International Outgoing Fellowship within the 7th European Community Framework Program (328162). SL, MNR and JGB were funded by the Microbio-E A*MIDEX project (ANR-11-IDEX-0001-02). This work was supported in part by the CNRS and the French Infrastructure for Integrated Structural Biology (FRISBI) ANR-10-INSB-05-01. NL and BH were supported by Agence Française de l'Environnement et de la Maîtrise de l'Energie (1201C102). PHW, GJD and LC thank the UK Biotechnology and Biological Sciences Research Council (BB/L001926/1 and BB/L021633/1) for funding. GJD is the Royal Society Ken Murray Research Professor.

Author contributions. MC and SL contributed equally to this work. MC identified the new enzymes and performed biochemical characterization. MNR was in charge of transcriptomic and proteomic analyses. MC, SL, SG, IG and MH performed production of proteins in flasks and bioreactors. FC performed ICP-MS analysis. SL and SG performed synergy assays with xylanase and protein crystallization. SL and GS solved the crystal structure. BH and NL performed bioinformatic analyses. MC, SL, SG performed HPAEC analyses. MF, DR and HR identified oxidized products using mass spectrometry. MC, SG and IG performed saccharification assays. AV, CM and BC carried out microscopy and NMR analyses. LC performed the EPR study under the direction of PHW and GJD. JGB supervised the work and organized the data. The manuscript was written by JGB with contributions from BH and PHW. All authors made comments on the manuscript and approved the final version. Figures were prepared by JGB, KEF, AL, NL, SL, LC, MF, SG and IG.

Competing Financial Interests Statement. The authors declare no competing financial interests.

252

253

References

1. Field, C. B., Behrenfeld, M. J., Randerson, J. T. & Falkowski, P. Primary production of the biosphere: integrating terrestrial and oceanic components. *Science* **281**, 237-240 (1998)
2. Himmel, M. E. *et al.* Biomass recalcitrance: engineering plants and enzymes for biofuels production. *Science* **315**, 804-807 (2007)
3. Biely, P., Singh, S. & Puchart, V. Towards enzymatic breakdown of complex plant xylan structures: State of the art. *Biotechnol. Adv.* **34**, 1260-1274 (2016)
4. Simmons, T. J. *et al.* Folding of xylan onto cellulose fibrils in plant cell walls revealed by solid-state NMR. *Nat. Commun.* **7**, 13902 (2016)
5. Loqué, D., Scheller, H. V. & Pauly, M. Engineering of plant cell walls for enhanced biofuel production. *Curr. Opin. Plant Biol.* **25**, 151-161 (2015)
6. Hibbett, D. S. & Donoghue, M. J. Analysis of character correlations among wood decay mechanisms, mating systems, and substrate ranges in homobasidiomycetes. *Syst. Biol.* **50**, 215-242 (2001)
7. Lombard, V., Golaconda Ramulu, H., Drula, E., Coutinho, P. M. & Henrissat, B. The carbohydrate-active enzymes database (CAZy) in 2013. *Nucleic Acids Res.* **42**, D490-495 (2014)
8. Riley, R. *et al.* Extensive sampling of basidiomycete genomes demonstrates inadequacy of the white-rot/brown-rot paradigm for wood decay fungi. *Proc. Natl. Acad. Sci. U.S.A.* **111**, 9923-9928 (2014)
9. Vaaje-Kolstad, G. *et al.* An oxidative enzyme boosting the enzymatic conversion of recalcitrant polysaccharides. *Science* **330**, 219-222 (2010)
10. Quinlan, R. J. *et al.* Insights into the oxidative degradation of cellulose by a copper metalloenzyme that exploits biomass components. *Proc. Natl. Acad. Sci. U.S.A.* **108**, 15079-15084 (2011)
11. Kracher, D. *et al.* Extracellular electron transfer systems fuel cellulose oxidative degradation. *Science* **352**, 1098-1101 (2016)

- 278 12. Johansen, K. S. Discovery and industrial applications of lytic polysaccharide mono-oxygenases.
279 *Biochem. Soc. Trans.* **44**, 143-149 (2016)
- 280 13. Hemsworth, G. R., Henrissat, B., Davies, G. J. & Walton, P. H. Discovery and characterization of a
281 new family of lytic polysaccharide monooxygenases. *Nat. Chem. Biol.* **10**, 122-126 (2014)
- 282 14. Vu, V. V., Beeson, W. T., Span, E. A., Farquhar, E. R. & Marletta, M. A. A family of starch-active
283 polysaccharide monooxygenases. *Proc. Natl. Acad. Sci. U.S.A.* **111**, 13822-13827 (2014)
- 284 15. Lo Leggio, L. *et al.* Structure and boosting activity of a starch-degrading lytic polysaccharide
285 monooxygenase. *Nat. Commun.* **6**, 5961 (2015)
- 286 16. Couturier, M. *et al.* Enhanced degradation of softwood versus hardwood by the white-rot fungus
287 *Pycnoporus coccineus*. *Biotechnol. Biofuels* **8**, 216 (2015)
- 288 17. Frandsen, K. E. *et al.* The molecular basis of polysaccharide cleavage by lytic polysaccharide
289 monooxygenases. *Nat. Chem. Biol.* **12**, 298-303 (2016)
- 290 18. Peisach, J. & Blumberg, W. E. Structural implications derived from the analysis of electron
291 paramagnetic resonance spectra of natural and artificial copper proteins. *Arch. Biochem. Biophys.*
292 **165**, 691-708 (1974)
- 293 19. Garajova, S. *et al.* Single-domain flavoenzymes trigger lytic polysaccharide monooxygenases for
294 oxidative degradation of cellulose. *Sci. Rep.* **6**, 28276 (2016)
- 295 20. Bennati-Granier, C. *et al.* Substrate specificity and regioselectivity of fungal AA9 lytic
296 polysaccharide monooxygenases secreted by *Podospora anserina*. *Biotechnol. Biofuels* **8**, 90 (2015)
- 297 21. Herpoël-Gimbert, I. *et al.* Comparative secretome analyses of two *Trichoderma reesei* RUT-C30 and
298 CL847 hypersecretory strains. *Biotechnol. Biofuels* **1**, 18 (2008)
- 299 22. Westereng, B. *et al.* Enzymatic cellulose oxidation is linked to lignin by long-range electron transfer.
300 *Sci. Rep.* **5**, 18561 (2015)
- 301 23. Villares, A. *et al.* Lytic polysaccharide monooxygenases disrupt the cellulose fibers structure. *Sci.*
302 *Rep.* **7**, 40262 (2017)

- 303 24. Frommhagen, M. *et al.* Discovery of the combined oxidative cleavage of plant xylan and cellulose by
304 a new fungal polysaccharide monooxygenase. *Biotechnol. Biofuels* **8**, 101 (2015)
- 305 25. Fanuel, M. *et al.* The *Podospora anserina* lytic polysaccharide monooxygenase PaLPMO9H
306 catalyzes oxidative cleavage of diverse plant cell wall matrix glycans. *Biotechnol. Biofuels* **10**, 63
307 (2017)
- 308 26. McCartney, L. *et al.* Differential recognition of plant cell walls by microbial xylan-specific
309 carbohydrate-binding modules. *Proc. Natl. Acad. Sci. U.S.A.* **103**, 4765-4770 (2006)
- 310 27. Nieduszynski, I. & Marchessault, R. H. Structure of beta-D-(1-->4')xylan hydrate. *Nature* **232**, 46-47
311 (1971)

312

Figure legends

Figure 1. Phylogeny of the AA14 family of LPMOs. Phylogenetic tree of 283 fungi analyzed for AA14 members. The number of AA14 in fungal species (listed in **Supplementary Data Set 1**) is represented by red bars (the scale is indicated at the bottom of the figure). When available, the mode of wood decay (brown-rots or white-rots) is specified next to the leaves of the tree. Pictures illustrate the taxonomical diversity of wood-decaying fungi displaying AA14 LPMOs; Genus (order) from top to bottom: *Xylaria* (Xylariales), *Trichoderma* (Hypocreales), *Nectria* (Hypocreales), *Tremella* (Hypocreales), *Pycnoporus* (Polyporales), *Ganoderma* (Polyporales), *Serpula* (Boletales), *Gymnopilus* (Agaricales). Photo credit: C. Lechat (AscoFrance) and A. Favel (CIRM-CF).

Figure 2. Structure of AA14 LPMO and organization of the copper active site. (a) Overall three-dimensional structure of *PcAA14B* (ribbon depiction with active site residues shown as sticks under transparent surface). (b) Active site (Histidine brace) overlay of Cu-*LsAA9A* (magenta) and *PcAA14B* (gold). (c) Continuous wave X-band EPR spectrum (9.3 GHz, 165 K) with simulation (red) of *PcAA14A*. More data are presented in **Supplementary Figures 5 and 6**.

Figure 3. Contribution of *PcAA14* enzymes to the saccharification of biomass. (a) Glucose release upon saccharification of pretreated pine and poplar by the CL847 *Trichoderma reesei* enzyme cocktail in the presence of *PcAA14A* or *PcAA14B* and ascorbic acid. Glucose was quantified using ionic chromatography. More saccharification assays are presented in **Supplementary Figure 8**. (b) Dose effect of the addition of *PcAA14A* on the saccharification of

pretreated pine. Concentration of *PcAA14A* was 0.1 μ M (+), 0.5 μ M (++) and 1 μ M (+++). Error bars indicate standard error of the mean from triplicate independent experiments. Data points are shown as dots.

Figure 4. Enzymatic activity of *PcAA14* LPMOs. (a) Morphology of birchwood cellulosic fibers treated with *PcAA14A* and *PcAA14B* LPMOs. Images were recorded after dispersion. Images are representative of the samples analyzed. (b) Solid state ^{13}C CP/MAS NMR analysis of LPMO-treated cellulosic fibers. The differences in hemicellulose content in enzyme-treated fibers were calculated from the C-1 and C-4 region deconvolution of NMR spectra and are indicated in **Supplementary Figure 10**. (c) Assays in the presence of a GH11 xylanase were performed on birchwood cellulose fibers. Xylobiose (X2) and xylotriose (X3) were quantified by ionic chromatography. Error bars indicate standard error of the mean from triplicate independent experiments. (d) Mass spectrometry identification of the X3 oxidized species detected at 429.13 m/z generated from birchwood cellulosic fibers by *PcAA14A* in synergy with a GH11 xylanase. The fragmentation pattern corresponds to a C1 oxidized species with an aldonic acid at the reducing end. ∇ : water losses. \square : H_2CO losses. An expanded view of the spectrum is provided in **Supplementary Figure 12**.

On-line Materials and Methods

Transcriptomics and secretomics of *Pycnoporus* sp.

Transcriptomic and proteomic data of three-days-old cultures of *Pycnoporus coccineus* BRFM 310 and *Pycnoporus sanguineus* BRFM 1264 grown on cellulose (Avicel), wheat straw, pine and aspen are described in^{16,28}.

Bioinformatic analysis of AA14 LPMOs

P. coccineus AA14 sequences (Genbank ID KY769369 and KY769370) were compared to the NCBI non redundant sequence database using BlastP²⁹ in February 2016. Blast searches conducted with AA14 did not retrieve AA9s, AA10s, AA11s or AA13s with significant scores, and vice-versa. MUSCLE³⁰ was used to perform multiple alignments. To avoid interference from the presence or absence of additional residues, the signal peptides and C-terminal extensions were removed. Bioinformatic analyses were performed on 286 fungal genomes sequenced and shared by JGI collaborators. Protein clusters are available thanks to the JGI (<https://goo.gl/ZAA2NX>) for each of these fungi. A phylogenetic tree has been inferred using 100 cleaned and merged alignments of proteins from selected clusters of proteins. Those clusters are present, as much as possible, in all fungi in 1 copy in order to maximize the score $\sum 1/n$ (with n, the number of copy in the genome). Sequences from clusters were aligned with Mafft³¹, trimmed with Gblocks³² and a phylogenetic tree was built with concatenation of alignments with Fasttree³³. The tree is displayed with Dendroscope³⁴ and Bio::phylo³⁵.

Production of *P.coccineus* AA14 LPMOs

The sequences corresponding to *PcAA14A* (Genbank ID KY769369) and *PcAA14B* (Genbank ID KY769370) genes from *P. coccineus* BRFM310 were synthesized after codon optimization for

expression in *P. pastoris* (GenScript, Piscataway, USA). The region corresponding to the native signal sequence was kept while the C-terminal extension region was removed. Synthesized genes were further inserted with into a modified pPICZαA vector (Invitrogen, Cergy-Pontoise, France) using *Bst*BI and *Xba*I restriction sites in frame with the (His)₆-tag located at the C-terminus of recombinant proteins. Fusion of *PcAA14A* with CBM1 was carried using the CBM1 domain of *PaLPMO9E*, which was added to *PcAA14A* at the end of the catalytic module using the linker sequence of *PaLPMO9E*²⁰. Constructs without (His)₆-tag sequence were also designed by adding a stop codon at the end of the AA14 catalytic module. *P. pastoris* strain X33 and the pPICZαA vector are components of the *P. pastoris* Easy Select Expression System (Invitrogen), all media and protocols are described in the manufacturer's manual (Invitrogen).

Transformation of competent *P. pastoris* X33 was performed by electroporation with *Pme*I-linearized pPICZαA recombinant plasmids and zeocin-resistant *P. pastoris* transformants were screened for protein production as described in³⁶. The best-producing transformants were grown in 2 L of BMGY medium containing 1 mL.L⁻¹ *Pichia* trace minerals 4 (PTM₄) salts in shaken flasks at 30°C in an orbital shaker (200 rpm) to an OD₆₀₀ of 2 to 6. Cells were then transferred to 400 mL of BMMY medium containing 1 mL.L⁻¹ of PTM₄ salts at 20°C in an orbital shaker (200 rpm) for 3 days, with supplementation of 3% (v/v) methanol every day.

Bioreactor productions were carried out in 1.3-L New Brunswick BioFlo[®] 115 fermentors (Eppendorf, Hamburg, Germany) following the *P. pastoris* fermentation process guidelines (Invitrogen). Recombinant enzymes were secreted up to ~1 g.L⁻¹ (**Supplementary Figure 13**).

Purification of *PcAA14* LPMOs

The culture supernatants were recovered by pelleting the cells by centrifugation at 2,700 g for 5 min, 4°C and filtered on 0.45 µm filters (Millipore, Molsheim, France). For (His)₆-tagged enzymes, the pH was adjusted to 7.8 and the supernatants were loaded onto 5 ml His Trap HP columns (GE healthcare, Buc, France) connected to an Akta Xpress system (GE healthcare). Prior to loading, the columns were equilibrated in 50 mM Tris HCl pH 7.8; 150 mM NaCl (buffer A). The loaded columns were then washed with 5 column volumes (CV) of 10 mM imidazole in buffer A, before the elution step with 5 CV of 150 mM imidazole in buffer A. Fractions containing the protein were pooled and concentrated with a 3-kDa vivaspin concentrator (Sartorius, Palaiseau, France) before loading onto a HiLoad 16/600 Superdex 75 Prep Grade column (GE Helthcare) and separated in 50 mM sodium acetate buffer pH 5.2. Gel filtration analysis showed that both *PcAA14* proteins are monomeric in solution. For enzymes without (His)₆-tag, salts contained in the culture media were diluted ten-fold in 20 mM Tris-HCl pH 8, then culture supernatants were concentrated with a Pellicon-2 10-kDa cutoff cassette (Millipore) to a volume of approx. 200 mL and loaded onto a 20-mL High Prep DEAE column (GE Helthcare). Proteins were eluted using a linear gradient of 1 M NaCl (0 to 700 mM in 200 mL). Fractions were then analyzed by SDS PAGE and those containing the recombinant protein were pooled and concentrated. The concentrated proteins were then incubated with one-fold molar equivalent of CuSO₄ overnight before separation on a HiLoad 16/600 Superdex 75 Prep Grade column in 50 mM sodium acetate buffer pH 5.2.

Biochemical analysis of AA14 LPMOs

Concentration of purified proteins was determined by using the Bradford assay (Bio-Rad, Marnes-la-Coquette, France) or using a nanodrop ND-2000 device with calculated molecular mass and molar extinction coefficients derived from the sequences. Proteins were loaded onto

10% SDS-PAGE gels (Thermo Fisher Scientific, IL, USA) which were stained with Coomassie Blue. The molecular mass under denaturing conditions was determined with reference standard proteins (Page Ruler Prestained Protein Ladder, Thermo Fisher Scientific). Native IEF was carried out in the Bio-Rad gel system, using pI standards ranging from 4.45 to 8.2 (Bio-Rad).

N-terminal amino acid sequence determination

The N-terminal amino acid sequences of purified *PcAA14A* and *PcAA14B* were determined according to the Edman degradation. Samples were electroblotted onto a polyvinylidene difluoride membrane (iBlot, Life Technologies). Analyses were carried out on a Procise Sequencing System (ThermoFisher).

Matrix-assisted laser desorption ionization/mass spectrometry

Matrix-assisted laser desorption ionization mass spectra analyses were performed on a Microflex II mass spectrometer (Bruker Daltonics). One μL of matrix [10 mg of 2,5-dihydroxybenzoic acid in 1 mL of $\text{CH}_3\text{CN}/\text{H}_2\text{O}$ 50/50 (v/v), 0.1% formic acid (v/v)] was added to 1 μL of intact *PcAA14A* or *PcAA14B* protein sample (100 pmoles) in the same solution. Then, mixtures were allowed to dry at room temperature. Data acquisition was operated using the Flex control software. External mass calibration was carried out on Peptide calibration standard (Bruker Daltonics).

Deglycosylation assays

To remove N-linked glycans, purified enzymes were treated with EndoHf (New England Biolabs, Ipswich, MA) under denaturing conditions according to the manufacturer's instructions. Briefly, 10 μg of protein were incubated in 0.5% SDS and 40 mM DTT and heated for 10 min at 100°C for complete denaturation. Denaturated samples were subsequently incubated with 1,500

441 units of EndoHf in 50 mM sodium acetate pH 6.0 for 1 h at 37°C. Deglycosylated and control
442 samples were analyzed by SDS-PAGE.

443 **Amplex Red assay**

444 A fluorimetric assay based on Amplex Red and horseradish peroxidase was used as described
445 previously³⁷. The reaction (total volume 100 μ L, 30°C, 30 min) was measured in 50 mM sodium
446 acetate buffer pH 6.0 containing 50 μ M Amplex Red (Sigma-Aldrich, Saint-Quentin Fallavier,
447 France), 7.1 U.mL⁻¹ horseradish peroxidase, 0.2 to 4 μ M enzyme, and 50 μ M reductant, i.e.
448 ascorbate, *p*-coumaric acid, caffeic acid, cinapic acid, vanillic acid, menadione, L-cysteine,
449 tannic acid, syringic acid, gallic acid, 3-hydroxyanthranilic acid (3-HAA) and epigallocatechin
450 gallate in water and fluorescence was detected using an excitation wavelength of 560 nm and an
451 emission wavelength of 595 nm using a Tecan Infinite M200 plate reader (Tecan, Männedorf,
452 Switzerland). The specific activity was counted from H₂O₂ calibration curve, and the slope
453 (13,227 counts. μ mol⁻¹) was used to convert the fluorimeters' readout (counts.min⁻¹) into enzyme
454 activity.

455 **ICP/MS Analysis**

456 To obtain apo enzymes, 100 mM EDTA treatment was performed overnight. Prior to the
457 analysis, samples were mineralized in a mixture containing 2/3 of nitric acid (Sigma-Aldrich,
458 65% Purissime) and 1/3 of hydrochloric acid (Fluka, 37%, Trace Select) at 120°C. The residues
459 were diluted in ultra-pure water (2 mL) before ICP/MS analysis. The ICP-MS instrument was an
460 ICAP Q (ThermoElectron, Les Ullis, France), equipped with a collision cell. The calibration
461 curve was obtained by dilution of a certified multi-element solution (Sigma-Aldrich). Copper

concentrations were determined using Plasmalab software (Thermo-Electron), at a mass of interest $m/z=63$.

Saccharification assays

Wheat straw, pine and poplar biomass were pretreated under acidic conditions. Sugar composition was determined using the alditol acetate method.³⁸ Wheat straw consisted of 51.98 ± 2.02 % (w/v) glucose, 5.70 ± 0.23 % (w/v) xylose and 0.46 ± 0.04 % (w/v) arabinose. Pine consisted of 43.25 ± 1.34 % (w/v) glucose, 0.24 ± 0.01 % (w/v) xylose and 0.15 ± 0.02 % (w/v) arabinose. Poplar consisted of 50.85 ± 0.91 % (w/v) glucose, 0.39 ± 0.01 % (w/v) xylose and 0.07 ± 0.01 % (w/v) arabinose. The enzymatic treatments were carried out in sodium acetate buffer (50 mM, pH 5.2) in a final volume of 1 ml at 0.5% consistency (w d.m./v). The LPMO treatment was carried out sequentially with a CL847 *T. reesei* enzyme cocktail²¹ provided by IFPEN (Rueil-Malmaison, France). Each *PcAA14* enzyme was added to the substrate at a concentration of between 0.1 and 1 μ M in the presence or absence of 1 mM ascorbic acid for 72 h, followed by addition of 1 mg.g⁻¹ dry matter (d. m.) substrate of commercial cellulases from *T. reesei* for 24 h. Enzymatic treatments were performed in 2-ml tubes incubated at 45°C and 850 rpm in a rotary shaker (Infors AG, Switzerland). Then, samples were centrifuged at 14,000 g for 5 min at 4°C and the soluble fraction was heated for 10 min at 100°C to stop the enzymatic reaction. Glucose was quantified by high performance anion exchange chromatography coupled with amperometric detection (HPAEC-PAD) as described in²⁰.

Polysaccharides cleavage assays

Avicel was purchased from Sigma-Aldrich and lichenan (from Icelandic moss), curdlan, starch, barley β -1,3/1,4-glucan, konjac glucomannan, wheat arabinoxylan, tamarind xyloglucan were

484 purchased from Megazyme (Wicklow, Ireland). PASC was prepared from Avicel as described
485 previously²⁰ in 50 mM sodium acetate buffer pH 5.2. A similar protocol was used to prepare
486 swollen squid pen chitin provided by Dominique Gillet (Mahtani Chitosan, India).
487 Glucuronoxylans were extracted from birchwood as described previously³⁹.

488 All the cleavage assays contained between 0.5 and 1 μ M of *PcAA14s* in the presence of 1 mM
489 ascorbate and 0.1% (w/v) polysaccharides. The enzyme reactions were performed in 2-mL tubes
490 and incubated in a thermomixer (Eppendorf, Montesson, France) at 45°C and 850 rpm. After 16
491 h of incubation, samples were heated for 10 min at 100°C to stop the enzymatic reaction and then
492 centrifuged at 14,000 *g* for 15 min at 4°C to separate the soluble fraction from the remaining
493 insoluble fraction before determination of soluble products using HPAEC as described above
494 with oligosaccharides standards (Megazyme).

495 **Microscopy**

496 Aqueous dispersions of Kraft birchwood cellulosic fibers (kindly provided by Sandra Tapin,
497 FCBA, Grenoble, France) were adjusted to pH 5.2 with acetate buffer (50 mM) in a final
498 reaction volume of 5 mL. Each *PcAA14* enzyme was added to the fibers at a final concentration
499 of 20 mg.g⁻¹ in the presence of 1 mM of ascorbic acid. Enzymatic incubation was performed at
500 40 °C under mild agitation for 48 h. Samples were then dispersed by a Polytron PT 2100
501 homogenizer (Kinematica AG, Germany) for 3 min, and ultrasonicated by means of a QSonica
502 Q700 sonicator (20 kHz, QSonica LLC., Newtown, USA) at 350 W ultrasound power for 3 min
503 as described previously²³. The reference sample was submitted to the same treatment but it did
504 not contain the *PcAA14* enzyme. Birchwood cellulose fibers (reference and *PcAA14*-treated)
505 were deposited onto a glass slide and observed by a BX51 polarizing microscope (Olympus
506 France S.A.S.) with a 4 \times objective. Images were captured by a U-CMAD3 camera (Olympus

Japan). For the atomic force microscopy (AFM) experiments, samples were deposited onto mica substrates from fiber solutions at 0.1 g L^{-1} , and allowed to dry overnight. Topographical images on mica were registered by a Nanoscope III-A AFM (Bruker, Santa Barbara, US). The images were collected in tapping mode under ambient air conditions (temperature and relative humidity) using a monolithic silicon tip (RFESP, Bruker) with a spring constant of 3 N m^{-1} , and a nominal frequency of 75 kHz . Image processing was performed with the WSxM 5.0 software. For transmission electron microscopy (TEM) experiments, fiber solutions at 0.1 g L^{-1} in water were deposited on freshly glow-discharged carbon-coated electron microscope grids (200 mesh, Delta Microscopies, France) and the excess of water was removed by blotting. The sample was then immediately negatively stained with uranyl acetate solution (2%, w/v) for 2 min and dried after blotting. The grids were observed with a Jeol JEM 1230 TEM at 80 kV .

NMR spectroscopy

Solid state ^{13}C NMR experiments were performed on a Bruker Avance III 400 spectrometer operating at a ^{13}C frequency of 100.62 MHz using a 4 mm double-resonance (H/X) magic angle spinning (MAS) probe. Samples were dialyzed against ultrapure water (MWCO 12-14000) for 7 days to remove buffer, ascorbate and released soluble sugars. Experiments were conducted at room temperature at a MAS frequency of 9 kHz using a cross-polarization sequence (CP/MAS). The ^{13}C chemical shift was referenced using the carbonyl signal of glycine at 176.03 ppm . The cross polarization pulse sequence parameters were: $3.2 \mu\text{s}$ proton 90° pulse, 2.50 ms contact time at 67.5 kHz , and 10 s recycle time. Typically, the accumulation of $5,120$ scans was used. All spectra obtained were processed and analyzed using Bruker Topspin version 3.2. To determine the crystallinity and the general cellulose's morphology of the C-1 and C-4 region of the samples, we used the sophisticated approach⁴⁰ that is described in details in our previous work²³.

530 For the C1-region, this approach used three Lorentzian lines for the crystalline part (Cr (I α) and
531 Cr (I β)) and one Gaussian line for the less ordered cellulose (para-crystalline cellulose, PCr). For
532 the C-4 region, four lines for the crystalline part corresponding to crystalline and para-crystalline
533 (PCr) cellulose and three Gaussian lines for the amorphous part (accessible surfaces, AS, and
534 inaccessible surface, IAS) were used. The cellulosic fibers contained xylan, which was
535 considered in the spectral decomposition: in the C-1 region with one line at 101.4 ppm and in the
536 C-4 region with one broad line centered at 81.6 ppm.

537 **Synergy assays with xylanase**

538 Assays were run on the birchwood cellulose fibers used in microscopy and NMR experiments.
539 Fibers were grinded (< 0.18 mm particle size) and hydrated in water under stirring for 48 h prior
540 to enzymatic assays. One mL reaction volumes containing 0.5% (w/v) birchwood fibers were
541 incubated with 1 μ M of PcAA14s and 0.1 μ M of GH11 xylanase M4 (*Aspergillus niger*) from
542 Megazyme (reference E-XYAN4) in 10 mM sodium acetate pH 5.2 supplemented or not with
543 1 mM L-cysteine. Prior to the reaction, the GH11 xylanase was buffer exchanged with 10 mM
544 sodium acetate pH 5.2 using a PD-10 column (GE Helthcare) to remove any trace of ammonium
545 sulfate. Enzymatic reactions were performed in 2-mL tubes and incubated in a thermomixer
546 (Eppendorf, Montesson, France) at 45°C and 850 rpm for 24 h. Samples were then centrifuged at
547 14,000 *g* for 5 min at 4°C to separate the soluble fraction from the remaining insoluble fraction.
548 Proteins were removed from the soluble oligosaccharides fraction by filtering the supernatants
549 using Nanosep 3K Omega centrifugal devices (Pall corporation). Soluble oligosaccharides
550 generated were analyzed by HPAEC as described previously and mass spectrometry (see below)
551 using non-oxidized xylo-oligosaccharides (Megazyme) as standards. Corresponding C1-oxidized

standards (from DP2 to DP4) were produced from non-oxidized xylo-oligosaccharides by using purified *Pa*CDHB prepared as described previously.²⁰ All assays were carried out in triplicate.

Electrospray mass spectrometry (ESI-MS and MS/MS)

Experiments were performed on a Synapt G2Si high-definition mass spectrometer (Waters Corp., Manchester, UK) equipped with an Electrospray ion (ESI) source. Two types of mass measurements were performed on the samples: firstly, a mass profile was done on a mass range of 300-2000 m/z (M/S). Ions of interest were further isolated and fragmented by collision-induced dissociation in the transfer cell of the instrument (MS/MS). In these experiments, ion mobility (IM) was activated to reduce interference from sample impurities. IM was performed in a travelling-wave ion mobility (TWIM) cell. The gas flows were held at 180 mL.min⁻¹ He in the helium cell and at 90 mL.min⁻¹ N₂ in the mobility cell. The IM traveling wave height was set to 40 V and its wave velocity was set to 480 m.s⁻¹ for positive ionization mode and 500 m.s⁻¹ for negative ionization mode. Samples were diluted 10-fold in MeOH/H₂O (1:1, v/v) and infused at a flow rate of 5 μ L.min⁻¹ in the instrument. The instrument was operated in positive or negative polarity, and in “sensitivity” mode.

Crystallization, data collection, structure determination and refinement

All crystallization experiments were carried out at 20°C by the sitting-drop vapour-diffusion method using 96-well crystallization plates (Swissci) and a Mosquito[®] Crystal (TTP labtech) crystallization robot. Reservoirs consisted of 40 μ L of commercial screens and crystallization drops were prepared by mixing 100 nL reservoir solution with 100, 200 and 300 nL of protein solution. An initial hit was obtained after 1 week from a condition of the AmSO₄ screen (Qiagen) consisting of 2.4 M (NH₄)₂SO₄ and 0.1 M citric acid pH 4.0. This condition was further

574 optimized to obtain diffraction-grade crystals by mixing protein solution at 28 mg mL⁻¹ with
575 precipitant solution consisting of 2.4 M (NH₄)₂SO₄ and 0.1 M citric acid pH 4.4 at a volume ratio
576 of 3:1. *PcAA14B* crystals grew to dimensions of 0.15×0.15×0.05 mm in one week. Crystals
577 belong to space group P4₁2₁2 with cell axes 204×204×110 Å and two molecules *per* asymmetric
578 unit.

579 Crystals of *PcAA14B* were soaked for 5 min in a solution where 2.4 M (NH₄)₂SO₄ of the mother
580 liquor was replaced by 2.4 M Li₂SO₄ for the sake of cryoprotection prior to flash-cooling in
581 liquid nitrogen. As X-ray fluorescence scans on native crystals did not reveal a significant
582 presence of copper within the crystals, a heavy atom derivative was prepared by soaking the
583 crystals in reservoir solution supplemented with 55 mM of the gadolinium complex gadoteridol
584 prior to cryo-cooling. Native diffraction data were collected on beamline ID23-1, while a MAD
585 dataset at wavelengths of 1.711 and 1.698 Å for peak/inflection and remote energies, was
586 collected on beamline ID30B at the European Synchrotron Radiation Facility (ESRF), Grenoble,
587 France. Data were indexed and integrated in space group P4₁2₁2 using XDS⁴¹ and subsequent
588 processing steps were performed with the CCP4 software suite⁴². Determination of the Gd³⁺
589 substructure and subsequent phasing combined with solvent flattening were carried out with
590 SHELXC/D/E⁴², leading to a pseudo-free correlation coefficient of 71.8%. Starting from
591 experimental phases, an initial model comprising 526 residues (out of 584), was automatically
592 built with Buccaneer⁴³ and manually completed with Coot⁴⁴. This initial model was used for
593 rigid body refinement followed by restrained refinement against native data with the program
594 Refmac⁴⁵. A random set of 5% of reflections was set aside for cross-validation purposes. Model
595 quality was assessed with internal modules of Coot⁴⁴ and using the Molprobit server⁴⁶. Figures
596 representing structural renderings were generated with the PyMOL Molecular Graphics System

(DeLano, W.L. The PyMOL Molecular Graphics on <http://www.pymol.org/>). Atomic coordinates and structure factors have been deposited within the Protein Data Bank <http://www.rcsb.org>⁴⁷. Data collection and refinement statistics are summarized in **Supplementary Table 4**.

EPR

Continuous wave (cw) X-band frozen solution EPR spectra of a 0.2 to 0.3 mM solution of Cu(II)-*PcAA14A* and *PcAA14B*, prepared and copper loaded as described above, in 10% v/v glycerol at pH 5.2 (50 mM sodium acetate buffer) and 165 K were acquired on a Bruker EMX spectrometer operating at ~9.30 GHz, with modulation amplitude of 4 G, modulation frequency 100 kHz and microwave power of 10.02 mW (4 scans). Both enzymes showed identical EPR spectra. Cw Q-band frozen solution spectra of 1.0 mM solution of Cu(II)- *PcAA14A* at pH 5.2 (50 mM sodium acetate buffer) and 113 K were acquired on a Jeol JES-X320 spectrometer operating at ~34.7 GHz, with modulation width 1 mT and microwave power of 1.0 mW (8 scans).

Spectral simulations were carried out using EasySpin 5.0.3⁴⁸. Simulation parameters are given in **Supplementary Table 3**. g_z and $|A_z|$ values were determined accurately from the absorptions at low field. It was assumed that g and A tensors were axially coincident. Accurate determination of the g_x , g_y , $|A_x|$ and $|A_y|$ was obtained by simultaneous fitting of both X and Q band spectra. The superhyperfine coupling values for the nitrogen atoms could not be determined accurately, although it was noted that satisfactory simulation could only be achieved with the addition of two nitrogen atoms with coupling in the range 30-36 MHz.

Statistics

For all statistics, $n = 3$ values were used to calculate the standard error of the mean. Values resulted from independent experiments. For all representative results, experiments were repeated at least two times and at least 20 images were collected for microscopy analyses.

Accession codes

PcAA14A and *PcAA14B* sequences were deposited in GenBank under accession numbers KY769369 and KY769370, respectively. The X-ray structure of *PcAA14B* was deposited in the Protein Data Bank with accession 5NO7. Raw EPR data are available on request through the Research Data York (DOI: 10.15124/8758d712-1e67-467e-b0f0-f0dd99f0232a).

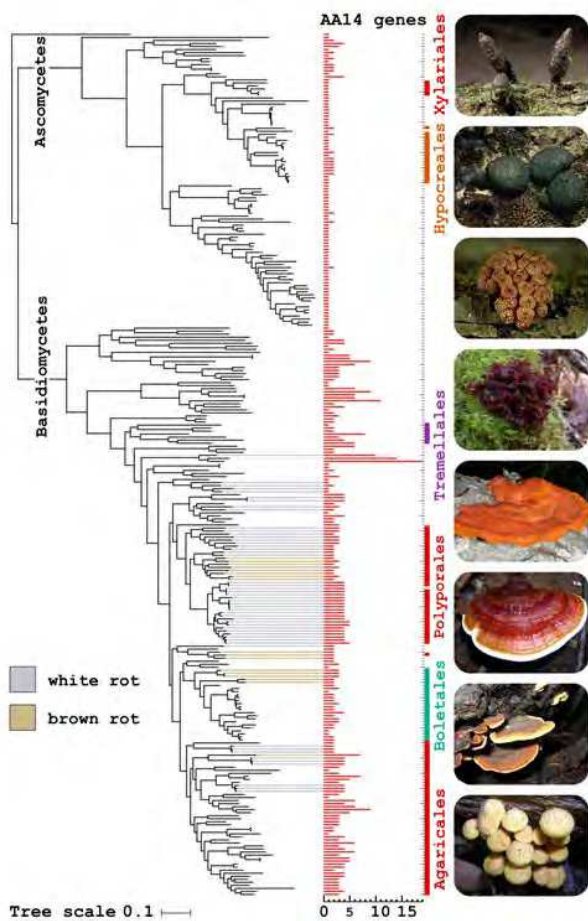
Data Availability Statement

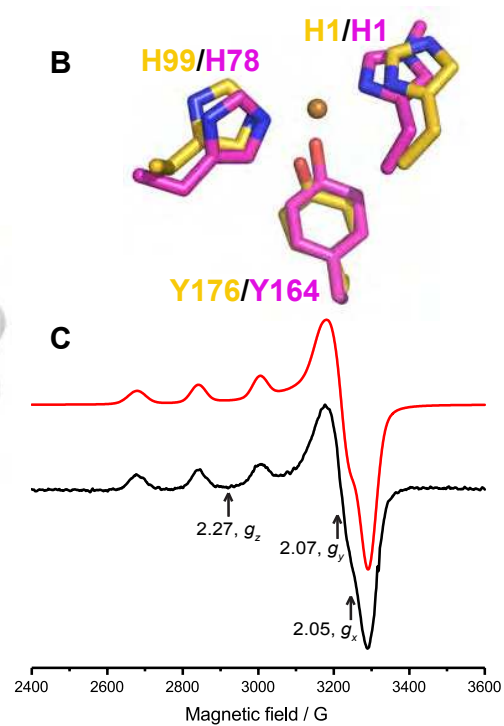
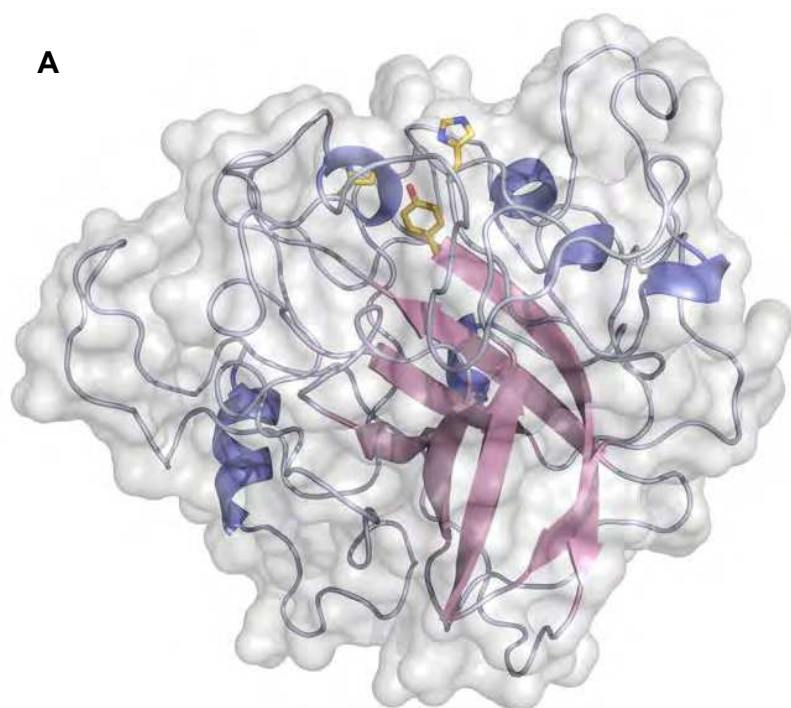
All data generated or analysed during this study are included in this published article (and its supplementary information files).

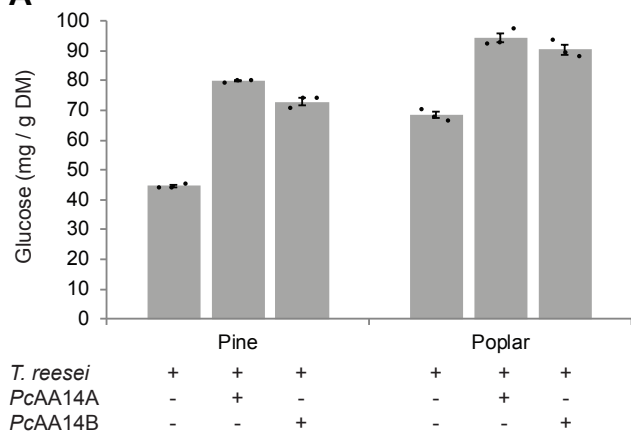
Methods-only references

28. Miyauchi, S. *et al.* Visual Comparative Omics of Fungi for Plant Biomass Deconstruction. *Front. Microbiol.* **7**, 1335 (2016)
29. Altschul, S. F., Gish, W., Miller, W., Myers, E. W. & Lipman, D. J. Basic local alignment search tool. *J. Mol. Biol.* **215**, 403-410 (1990)
30. Edgar, R. C. MUSCLE: multiple sequence alignment with high accuracy and high throughput. *Nucleic Acids Res.* **32**, 1792-1797 (2004)
31. Katoh, K. & Standley, D. M. MAFFT multiple sequence alignment software version 7: improvements in performance and usability. *Mol. Biol. Evol.* **30**, 772-780. (2013)
32. Talavera, G. & Castresana, J. Improvement of phylogenies after removing divergent and ambiguously aligned blocks from protein sequence alignments. *Syst. Biol.* **56**, 564-577 (2007)
33. Price, M. N., Dehal, P. S. & Arkin, A. P. FastTree 2--approximately maximum-likelihood trees for large alignments. *PLoS One* **5**, e9490 (2010)

34. Huson, D. H. & Scornavacca, C. Dendroscope 3: an interactive tool for rooted phylogenetic trees and networks. *Syst. Biol.* **61**, 1061-1067 (2012)
35. Vos, R. A., Caravas, J., Hartmann, K., Jensen, M.A. & Miller, C. BIO:Phylo-phyloinformatic analysis using perl. *BMC Bioinformatics* **12**, 632011 (2011)
36. Haon, M. *et al.* Recombinant protein production facility for fungal biomass-degrading enzymes using the yeast *Pichia pastoris*. *Front. Microbiol.* **6**, 1002 (2015)
37. Kittl, R., Kracher, D., Burgstaller, D., Haltrich, D. & Ludwig, R. Production of four *Neurospora crassa* lytic polysaccharide monooxygenases in *Pichia pastoris* monitored by a fluorimetric assay. *Biotechnol. Biofuels* **5**, 79 (2012)
38. Englyst, H.N. & Cummings, J.H. Improved method for measurement of dietary fiber as non-starch polysaccharides in plant foods. *J. Assoc. Off. Anal. Chem.* **71**, 808-814 (1988)
39. Westbye, P., Svanberg, C. & Gatenholm, P. The effect of molecular composition of xylan extracted from birch on its assembly onto bleached softwood kraft pulp. *Holzforschung* **60**, 143-148 (2006)
40. Larsson, P. T., Wickholm, K. & Iversen, T. A CP/MAS ¹³C NMR investigation of molecular ordering in celluloses. *Carbohydrate Research* **302**, 19-25 (1997)
41. Kabsch, W. XDS. *Acta Crystallogr. D Biol. Crystallogr.* **66**, 125-132 (2010)
42. Winn, M. D. *et al.* Overview of the CCP4 suite and current developments. *Acta Crystallogr. D Biol. Crystallogr.* **67**, 235-242 (2011)
43. Cowtan, K. The Buccaneer software for automated model building. 1. Tracing protein chains. *Acta Crystallogr. D Biol. Crystallogr.* **62**, 1002-1011 (2006)
44. Emsley, P., Lohkamp, B., Scott, W. G. & Cowtan, K. Features and development of Coot. *Acta Crystallogr. D Biol. Crystallogr.* **66**, 486-501 (2010)
45. Murshudov, G. N., Vagin, A. A. & Dodson, E. J. Refinement of macromolecular structures by the maximum-likelihood method. *Acta Crystallogr. D Biol. Crystallogr.* **53**, 240-255 (1997)
46. Chen, V. B. *et al.* MolProbity: all-atom structure validation for macromolecular crystallography. *Acta Crystallogr. D Biol. Crystallogr.* **66**, 12-21 (2010)
47. Berman, H., Henrick, K. & Nakamura, H. Announcing the worldwide Protein Data Bank. *Nat. Struct. Biol.* **10**, 980 (2003)
48. Stoll, S. & Schweiger, A. EasySpin, a comprehensive software package for spectral simulation and analysis in EPR. *J. Magn. Reson.* **178**, 42-55 (2006)





A**B**